Research Square

Preprints are preliminary reports that have not undergone peer review.
They should not be considered conclusive, used to inform clinical practice,
or referenced by the media as validated information.

Preparation of magnetic dendrimer and immobilization of laccase for dye removal

Tianwen Lu
Xi'an Polytechnic University
Yixuan Dai
Xi'an Polytechnic University
Yue Shi
Xi'an Polytechnic University
Xiaojun Wang
Xi'an Polytechnic University
Yinan Hong
Xi'an Polytechnic University
Hong Pan
441595837@qq.com
Xi'an Polytechnic University
Zhansheng Wu
Xi'an Polytechnic University

Research Article

Keywords: magnetic nanoparticles, Polyaminoamide (PAMAM) dendrimers, immobilized laccase, MO removal

Posted Date: May 12th, 2025

DOI: https://doi.org/10.21203/rs.3.rs-6529585/v1

License: This work is licensed under a Creative Commons Attribution 4.0 International License.
Read Full License

Additional Declarations: No competing interests reported.

Version of Record: A version of this preprint was published at BioNanoScience on July 2nd, 2025. See the published version at https://doi.org/10.1007/s12668-025-02057-4.

Preparation of magnetic dendrimer and immobilization of laccase for dye removal

Tianwen Lu[1], Yixuan Dai[1], Yue Shi[1], Xiaojun Wang[1], Yinan Hong[1], Hong Pan[1,*], Zhansheng Wu[1]

[1] School of Environmental and Chemical Engineering, Xi'an Key Laboratory of Textile Chemical Engineering Auxiliaries, Engineering Research Center of Biological Resources Development and Pollution Control Universities of Shaanxi Province, Key Laboratory of Textile Dyeing Wastewater Treatment Universities of Shaanxi Province, Xi'an Polytechnic University, Xi'an 710048, P.R. China

ABSTRACT

Laccase is a kind of green biocatalyst which is widely distributed in nature. However, the application of free laccase was greatly limited due to the poor stability and low utilization. In order to prepare a carrier with abundant immobilized sites, magnetic dendrimer (MPG-x) grafted by PAMAM was constructed using amino-functionalized Fe_3O_4 as divergent nucleus in this study. Then the immobilized laccase MPG-2@GA-Lac and MPG-2@Cu^{2+} -Lac were prepared by glutaraldehyde crosslinking and copper chelating adsorption, respectively. The results showed that the two immobilized laccases showed better comprehensive stability than free laccase. Moreover, the activation of Cu^{2+} in the active center of laccase made MPG-2@Cu^{2+} -Lac exhibit better stability. MPG-2@GA-Lac and MPG-2@Cu^{2+} -Lac retained 74.4% and 108.1% of the initial free laccase activity, respectively. Compared with MPG-2@GA-Lac, MPG-2@Cu^{2+} -Lac achieved better methyl orange (MO) removal over a wider pH and temperature range. This study is expected to further expand the application of laccase in the degradation of dye wastewater.

KEYWORDS: magnetic nanoparticles, Polyaminoamide (PAMAM) dendrimers, immobilized laccase, MO removal

Corresponding Author: Hong Pan.
Email Adress: 441595837@qq.com

1. INTRODUCTION

Laccase has been widely used in many fields such as food processing (1), biosensor (2), textile printing and dyeing wastewater treatment (3, 4) and biological bleaching (5). However, the application of free laccase was greatly limited due to the poor stability, low recycling efficiency and difficulty in separating from the reaction system (6). The emergence of enzyme immobilization technology had successfully solved these defects and greatly reduced the cost of application. Recently, an increasing variety of carriers and supports were used to immobilize enzyme, including chitosan (7), silica (8), nanotubes (9), metal-organic frameworks (MOFs) (10, 11), covalent organic frameworks (COFs) (12), magnetic materials (13) and dendritic polymers (14). Among many immobilized carriers, magnetic nanomaterials with unique magnetic properties and low biological toxicity (15) was used universally. However, magnetic nanomaterials often need to be modified to add more functionalization sites for binding and reducing the agglomeration. Ran et al. (16) prepared a magnetic nanocore with putaminal structure Fe_3O_4@MoS_2@PEI for laccase immobilization, whose loading capacity reached 120 mg/g, and the recovery rate of laccase activity reached 90%. Whatsmore, its degradation rate of carcinogenic organic pollutants in water was excellent. Li et al. (17) designed a functionalized

Fe_3O_4@C nanoparticles and chelated with Cu^{2+} to immobilize laccase under mild conditions, which showed good stability and dye degradation ability.

Polyamide-amine (PAMAM) dendrimer is a highly branched material composed of a central core, an internal "branch" and abundance outermost terminal groups (18). After modification, it can be used to encapsulate biological macromolecules (19), which was widely used in biopharmaceutical (20), drug delivery (21) and targeted therapy of cancer (22). Wang et al. (23) obtained an enzyme-facilitated nanogel carrier based on G-4 PAMAM dendrimer through covalent modification to achieve targeted drug delivery in cancer therapy. By repeated Michael addition and amidation reactions, dendritic polymers with different algebraic surfaces rich in rich in a large number of

amino groups can be obtained. Dendrimer with different surface functional groups can be obtained by further surface functionalization modification. Zhao et al. (24) used three kinds of amine reagents to graft dendrimers onto Fe_3O_4 to prepare different generations of Fe_3O_4@SiO_2/PAMAM magnetic nanoparticles. The results showed that the immobilized enzyme showed higher enzyme activity and environmental tolerance than the free enzyme. In addition, dendrimers can be used to immobilize metal ions to obtain efficient metal catalysts or to achieve the adsorption and removal of metal ions. Fan et al. (25) synthesized PEI-modified microcrystalline cellulose PAMAM dendritic macromolecules (MCC-PAMAM-G2.5-PEI) by covalent bonding as a new bimetallic catalyst for supporting Pd^{2+} and Cu^{2+} ions. Compared with other reported catalysts, the catalyst showed milder reaction conditions, shorter reaction time and higher yield. Sohail et al.(26) synthesized PAMAM dendrimers by divergence method to achieve efficient removal of metal nickel.

Although PAMAM dendrimers received extensive studies, there are few reports on the application of dendrimers in the immobilization of laccase. Hence, dendritic macromolecular nanocarriers with magnetic(Fe_3O_4@SiO_2-NH_2/PAMAM) were obtained by grafting different algebraic PAMAM dendrimer with magnetic Fe_3O_4 as core and surface amino functionalization, which were used for laccase immobilization. Crosslinking with and Cu^{2+}, the stability and reusability of two immobilized laccases at different temperatures and pH values were compared. Finally, the removal efficiency of the two immobilized laccase in methyl orange solution was determined, and the degradation performance was evaluated.

2. MATERIALS AND METHODS

2.1 Materials

Laccase was provided by SUNSON (Ningxia, China), Fe_3O_4, Tetraethyl silicate (TEOS), (3-aminopropyl) triethoxysilane (APTES), Methyl acrylate (MA), Diethylenetriamine (DETA), Iminodiacetic acid (IDA), Ammonia (25-28%),

Glutaraldehyde (50%), 2,2' -diazo-di-3-ethylbenzothiazolin-6-sulfonic acid (ABTS) were purchased from Aladdin Chemistry Co. Ltd (China). Methyl orange, Methanol, $CuSO_4 \cdot 5H_2O$, Anhydrous ethanol and Deionized water. All reagents were analytically pure and required no further purification.

2.2 Preparation of amino-functionalized magnetic nanoparticles (Fe3O4@SiO2-NH2)

Synthesis of Fe_3O_4@SiO_2-NH_2 based on the method described in a study by Chen et al. (27). 1.0 g of Fe_3O_4 was dispersed in 100 mL ethanol solution (80%), and Fe_3O_4 was uniformly dispersed by ultrasound. Then the ammonia of 2 mL was added to the system, and 2 mL TEOS was added slowly while stirring, then reacted at 25 ℃ for 12 h. The product was washed three times with 1:1 ethanol-aqueous solution to remove unreacted TEOS and the first reaction was finished. Subsequently, the product was dispersed in 100 mL ethanol solution (80%) again, 2 mL ammonia and 2 mL APTES was added successively while the solution was stirred continuously and reacted at 25 ℃ for 10 h. After washing with 1:1 ethanol-aqueous solution for several times, the surface amino modified magnetic nanoparticles were obtained after freeze-drying, which was named MPG-0.

2.3 Preparation of magnetic dendrimer nanocarriers (Fe3O4@SiO2-NH2/PAMAM)

Fe_3O_4@SiO_2-NH_2/PAMAM was synthesized according to methods described by Zhao et al.(24) and Unniganapathi et al.(28) with modification. The initial phase involves the Michael addition reaction. Initially, 0.5 g of MPG-0 was dispersed in 65 mL of methanol solution and subjected to ultrasonic dispersion for 20 minutes. The solution was then cooled in an ice bath, followed by the slow addition of 15 mL of MA, with continuous stirring maintained. The mixture was allowed to react at 35 ℃ for 24 hours. Subsequently, unreacted MA was removed by repeated methanol washing. The resultant half-generation product, obtained after freeze-drying, was designated as MPG-0.5.

The subsequent phase is the amidation reaction. For this step, 0.5 g of MPG-0.5 was dispersed in 55 mL of methanol solution and subjected to ultrasonic dispersion for 20 minutes. Thereafter, 25 mL of DETA solution was slowly added, with continuous stirring maintained, and the mixture was allowed to react at 35 ℃ for 24 hours. Unreacted DETA was removed by repeated washing with methanol solution, and the first generation product, obtained after freeze-drying, was labeled as MPG-1.

By repeating the aforementioned procedures and suitably increasing the amounts of MA and DETA added, as well as extending the reaction time and temperature, magnetic tree-shaped macromolecular nanocarriers with higher algebras can be synthesized. These are referred to as MPG-x, where "x" denotes the different generations.

2.4 Preparation of immobilized laccase

A 20mg quantity of MPG-x was uniformly dispersed within a glutaraldehyde solution of designated concentration. Following a cross-linking reaction, which was allowed to proceed for a specified duration, the magnetic nanoparticles were isolated using a magnetic field. Subsequently, the nanoparticles were washed multiple times with disodium hydrogen phosphate-citric acid buffer (hereinafter referred to as the buffer solution) to ensure the complete removal of any unreacted glutaraldehyde. Thereafter, varying concentrations of laccase solution were introduced, and the immobilized laccase was recovered using a magnetic field after an adequate period of time. The immobilized laccase was then rigorously washed with the buffer solution until no detectable laccase remained in the supernatant.

The construction of the copper ion chelate adsorption immobilized laccase was conducted according to Xia et al.(29). Initially, the surface of the carrier was carboxylated using a specific concentration of iminodiacetic acid, serving as a bridging agent. Subsequently, copper ions were affixed to the carrier surface through reaction with copper sulfate, thereby preparing the immobilized laccase via metal chelate adsorption.

2.5 Characterization

The morphology and size of the carrier were examined using a scanning electron microscope (ZEISS Sigma 300, Germany). For the analysis of the elements present in the material, an energy dispersive X-ray spectrometer (DES) and an organic element analyzer (Elementar Vario EL cube, Germany) were employed. Fourier transform infrared spectroscopy (FT-IR, Nicolet 5700) was utilized to determine the functional groups within the materials. The crystal structure of the materials was observed with an X-ray diffractometer (XRD, MiniFlex600, Angle range 10° to 80°). To assess the magnetic properties of the material, a vibrating sample magnetometer (VSM, LakeShore 8600, USA) was used. Thermogravimetric analysis was carried out by means of a thermogravimetric analyzer (TGA/SDTA851e MET 600W). Lastly, X-ray photoelectron spectroscopy (XPS, ULVAC-PHI.INC, PHI5000 VersaprobeIII) was applied to analyze the element composition.

2.6 Laccase activity and laccase loading assay

Laccase activity is defined as the quantity of laccase necessary to oxidize 1 μmol of ABTS within a unit of time. For the laccase activity assessment, a laccase sample (comprising 0.1 mL of free enzyme or 10 mg of immobilized laccase) was introduced into a buffer solution adjusted to a specific pH. The mixture was then incubated at the optimal temperature for a duration of 5 minutes. Subsequently, 0.3 mL of a 1 mM ABTS solution was added to initiate the reaction (resulting in a total system volume of 3 mL). The laccase activity was determined by quantifying the alteration in absorbance at a wavelength of 420 nm, measured before and after a 3-minute interval. The laccase activities for both free and immobilized laccase were calculated using Eq. 1, Eq. 2 and Eq. 3 (30, 31):

$$\text{Free laccase activity (U/mL)} = \frac{\Delta OD \times N \times V_T \times 1000}{\Delta t \times \varepsilon \times L \times V_L} \quad \text{Eq. 1}$$

$$\text{Expressed activity of immobilized laccase (U/g biocatalyst)} = \frac{\Delta OD \times V_T \times 1000}{\Delta t \times \varepsilon \times L \times M_0} \quad \text{Eq. 2}$$

$$\text{Specific activity of immobilized laccase (U/g protein)} = \frac{\Delta OD \times V_T \times 1000}{\Delta t \times \varepsilon \times L \times M_1} \quad \text{Eq. 3}$$

In this context, $\Delta OD/\Delta t$ is employed to denote the change in absorbance per unit time. V_T represents the total volume (mL) of the laccase reaction. V_L indicates the volume (mL) of the laccase solution added. The extinction coefficient of ABTS at 420 nm, denoted as ε (is 36000 $L \cdot mol^{-1} \cdot cm^{-1}$). M_0 refers to the mass (g) of the immobilized laccase. M_1 represents the protein content (g) of the immobilized laccase. L is the optical path (cm) through the colorimetric dish.

The relative activity is calculated using Eq. 4:

$$\text{Relative activity} = \frac{A_i}{A_{max}} \times 100\% \quad \text{Eq. 4}$$

In this context, A_i denotes the laccase activity measured per batch, expressed in units of U/g or U/mL. Meanwhile, A_{max} represents the maximum laccase activity measured per batch, also quantified in U/g or U/mL.

The protein content within the supernatant was assessed through the Coomassie brilliant blue method. The protein content is computed using Eq. 5:

$$\text{Laccase loading (mg/g)} = \frac{(C_0 - C_1) \times V}{m} \quad \text{Eq. 5}$$

Where C_0 represents the laccase concentration in the initial solution (expressed in mg/mL), C_1 denotes the laccase concentration in the supernatant following the reaction (expressed in mg/mL), and m signifies the mass of the carrier (measured in grams).

2.7 Study on the stability of immobilized laccase

The stability of both free and immobilized laccase was assessed by examining the effects of varying pH (ranging from 2.0 to 7.0) and temperature (spanning from 25 ℃ to 65 ℃) on laccase activity. Test samples underwent a 5-minute reaction under different conditions, after which laccase activity was quantified employing the aforementioned formula.

To evaluate the operational stability of immobilized laccase, the enzyme was

reacted in a buffer at its optimal temperature and pH for 5 minutes, followed by the addition of 1 mM ABTS to initiate the reaction. Upon completion, the immobilized laccase was isolated using a magnet, and residual $ABTS^{+}$ was removed with a buffer wash. Subsequently, fresh buffer and ABTS solution were added to commence the subsequent cycle.

The storage stability of free and immobilized laccase was investigated by storing them at 4 ℃ for a duration of 22 days. The maximum laccase activity exhibited by both free and immobilized forms was designated as 100% for comparative purposes.

2.8 Removal of MO by immobilized laccase

The degradation capacity of immobilized laccase was assessed employing MO as the substrate. Specifically, 20 mg of MPG-2@GA-Lac or MPG-2@Cu^{2+}-Lac was introduced into 10 mL of methyl orange aqueous solution, with concentrations ranging from 10 mg/L to 50 mg/L. Subsequently, 100 μL of ABTS (1 mM) was added to facilitate the reaction, which was then agitated under optimal conditions. At regular intervals, the supernatant was isolated, and its absorbance was measured at 463 nm using a UV-Vis spectrophotometer. Following this, the immobilized laccase was washed with buffer solution at its optimal pH, and 10 mL of MO aqueous solution was reapplied for subsequent degradation cycles. The entire degradation experiment was conducted over six cycles.

The removal efficiency was calculated as Eq. 6:

$$\text{Remove efficiency} = \frac{C_0 - C_1}{C_0} \times 100\% \qquad \text{Eq. 6}$$

Where C_0 represents the concentration of the initial methylene blue (MO) aqueous solution, and C_1 denotes the concentration of the MO aqueous solution after a certain reaction time.

In order to investigate the MO degradation efficiency of two immobilized laccases under different conditions, the degradation kinetics was analyzed systematically. The degradation kinetics models are expressed as Eq. 7:

$$\frac{C_t}{C_0} = e^{-kt} \qquad \text{Eq. 7}$$

Where C_t is the equilibrium concentration of MO at the reaction time t (mg/L); C_0 is the initial concentration of MO (mg/L); and k is the rate constant of pseudo-first-order kinetics.

3. RESULTS AND DISCUSSION

3.1 Characterization of magnetic dendrimer carriers and immobilized laccase

The SEM images of Fe_3O_4 before and after modification are presented in Fig.1. From Fig.1(A), it can be observed that Fe_3O_4 displays a spherical or ellipsoidal nanoparticle morphology, with a relatively pronounced agglomeration tendency. Fig.1 (B, C) depict the images of MPG-0 and MPG-2@Cu^{2+} respectively. It is evident that the modified magnetic materials remained the nanoscale. In comparison to Fe_3O_4, both MPG-0 and MPG-2@Cu^{2+} exhibit larger particle sizes, while the agglomeration phenomenon is also moderately improved (31). As illustrated in Fig.1(D, E), the presence of newly added elements C, N, and Si in the energy-dispersive X-ray spectroscopy (EDS) spectrum confirms the successful amino functionalization of the surface of Fe_3O_4 particles. Furthermore, the detection of the element Cu indicates the successful chelation of Cu^{2+}.

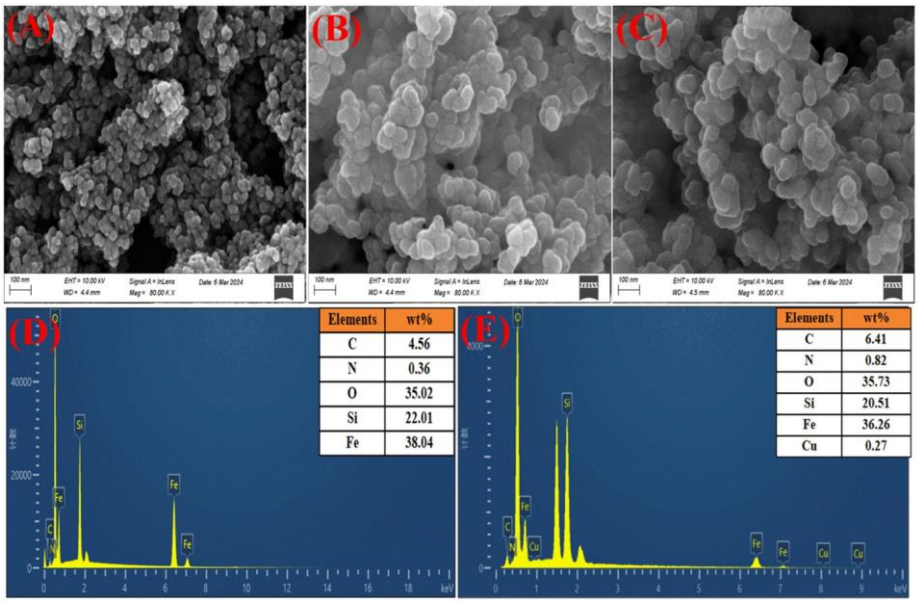


Fig.1. SEM of (A) Fe_3O_4, (B) MPG-0 and (C) MPG-2@Cu^{2+}, EDS of (D) MPG-0 and (E) MPG-2@Cu^{2+}.

.

(A) displays the FT-IR spectra of the magnetic particles. The peaks observed at 567 cm^{-1} for Fe_3O_4, MPG-0, and MPG-2 correspond to the characteristic absorption peaks of Fe-O, as reported by He et al. (32). The broad and prominent peaks at 3340 cm^{-1} are primarily attributed to the bending vibrations of N-H and the intermolecular hydrogen bonds of $-NH_2$. The peaks at 460 cm^{-1} for both MPG-0 and MPG-2 represent the characteristic absorption peaks of Fe-O-Si, suggesting the successful coating of SiO_2 on the surface of Fe_3O_4. The peaks at 1083 cm^{-1} and 956 cm^{-1} correspond to the symmetric and asymmetric bending modes of Si-O-Si, respectively, indicating the successful amino-functionalization modification on the surface of Fe_3O_4. Notably, new peaks at 1664 cm^{-1}, 1596 cm^{-1}, and 1439 cm^{-1} are clearly evident in MPG-2, which are associated with the stretching vibrations of the amide bond (C=O and C-N) and the bending vibration of N-H, respectively. These observations confirm the successful modification of the MPG-0 surface with polyamidoamine (PAMAM) dendrimers (33, 34).

The X-ray diffraction (XRD) patterns of Fe_3O_4, MPG-0, and MPG-2 are presented in Fig.2(B). The prominent peaks observed at 30.2°, 35.6°, 43.3°, 53.9°, 57.5°, and 63° correspond to the (220), (311), (400), (422), (511), and (440) crystal planes of Fe_3O_4 (PDF#98-000-0294), respectively, according to He et al.(32). Notably, in the XRD patterns of both MPG-0 and MPG-2, these peaks remain unshifted, suggesting that the surface functionalization of Fe_3O_4 and the subsequent PAMAM dendrimer modification do not alter the crystalline structure of the Fe_3O_4 particles.

The TGA results of the materials are presented in Fig.2(C). From 30 ℃ to 324 ℃, the weight loss of Fe_3O_4 was 5.07%, primarily attributed to the evaporation of water within Fe3O4. At 800 ℃, Fe_3O_4 exhibited a weight loss of 6.27%. The weight loss of MPG-0 at 800 ℃ (7.1%) was predominantly due to the thermal decomposition of the silane coupling agent on the surface of Fe_3O_4, thereby successfully confirming the aminofunctionalization of the Fe_3O_4 surface (with the silane coupling agent accounting

for approximately 0.83%). In comparison to MPG-0, MPG-1 and MPG-2 exhibited greater weight loss (approximately 8.07% and 8.51%, respectively), primarily due to the decomposition of their dendritic molecular structures caused by high temperatures (33), indicating the successful preparation of magnetic dendritic macromolecular carriers with different algebraic structures. The higher weight loss observed in MPG-2@GA-Lac and MPG-2@Cu^{2+}-Lac signifies the realization of laccase fixation on the carrier.

The magnetic properties of Fe_3O_4 before and after modification were examined utilizing a vibrating sample magnetometer. As depicted in Fig.2(D), the saturation magnetization of Fe_3O_4 attained 68.9 emu/g. Meanwhile, the modified magnetic nanoparticles MPG-0 and MPG-2 exhibited saturation magnetization values of 45.3 emu/g and 42.9 emu/g, respectively. This reduction in saturation magnetization serves to further substantiate the success of the functionalization modification and PAMAM dendrimer modification. Upon immobilizing laccase, the saturated magnetization of MPG-2@GA-Lac and MPG-2@Cu^{2+}-Lac decreased to 36.8 emu/g and 36.3 emu/g, respectively, signifying the successful immobilization of laccase on the surface of the carriers. Simultaneously, the high level of saturation magnetization facilitated the facile separation of the magnetic nanoparticles from the reaction system, thereby streamlining subsequent operations (34).

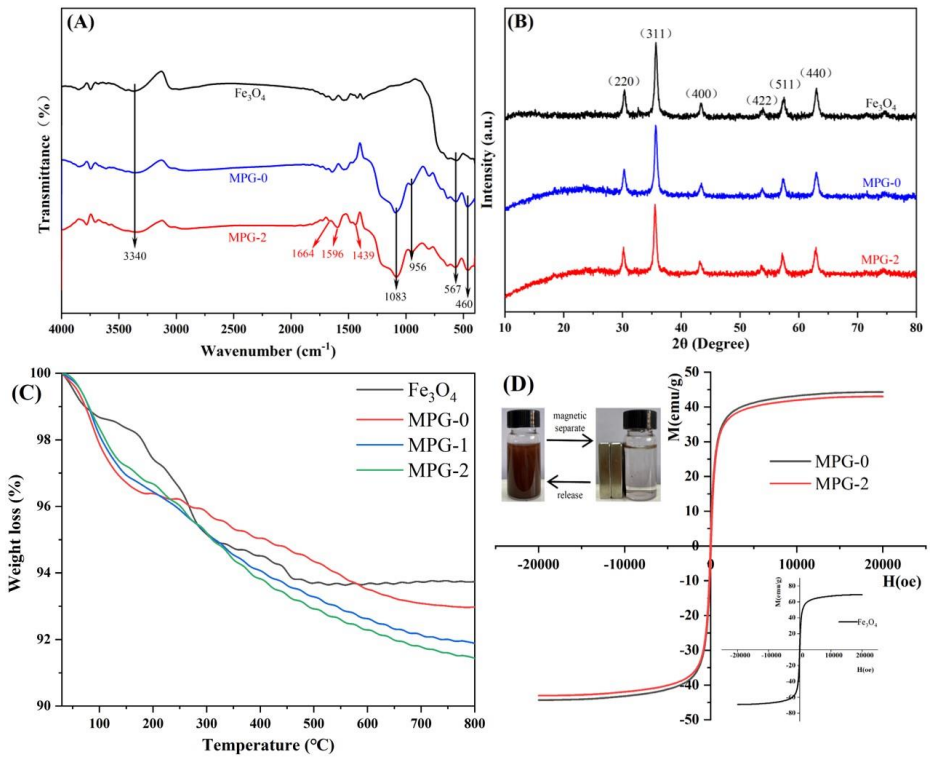


Fig.2. (A) FT-IR of Fe_3O_4, MPG-0 and MPG-2. (B) XRD patterns of Fe_3O_4, MPG-0 and MPG-2. (C) TGA analysis of Fe_3O_4, MPG-0, MPG-1, MPG-2, MPG-2@GA-Lac and MPG-2@Cu^{2+}-Lac. (D) Magnetization curves of Fe_3O_4, MPG-0, MPG-2, MPG-2@GA-Lac and MPG-2@Cu^{2+}-Lac.

The X-ray Photoelectron Spectroscopy (XPS) analysis of the magnetic nanoparticle MPG-2 is presented in Fig.3. Specifically, Fig.3(A) displays the complete spectrum of MPG-2, wherein elements such as C, O, N, Fe, and Si are all distinctly detectable. Referring to Fig.3(B), the peaks observed at 283.9 eV, 286.1 eV, and 287.2 eV within the C 1s region correspond to the C-C groups resulting from functionalization in MPG-2, as well as the C-N and C=O groups within the amide bonds of the PAMAM dendrimer, respectively. These findings corroborate the successful preparation of the modified magnetic nanoparticles.

In Fig.3(C), the three peaks identified in the O 1s spectrum are attributed to iron oxides (529.5 eV), SiO_2 (530.9 eV), and the C=O group (532.5 eV) within the PAMAM dendrimer. This confirms the successful coating with silica and modification with dendritic macromolecules. Similarly, Fig.3(D) reveals peaks at 397.9 eV and

399.8 eV within the N 1s region, which correspond to primary and secondary amines in the PAMAM dendrimer, respectively. This suggests that a substantial number of amino groups have been successfully grafted onto the surface of the magnetic nanocarriers.

In the Fe 2p spectrum of Fig.3(E), the peaks observed at 710.6 eV and 723.9 eV correspond to the characteristic peaks of the Fe 2p3/2 and Fe 2p1/2 oxidation states, respectively, which is consistent with the XPS patterns characteristic of known Fe_3O_4 materials (35). Lastly, the Si 2p spectrum in Fig.3(F) displays a single peak at 101.6 eV, which is confirmed to correspond to the Si-O-Si group.

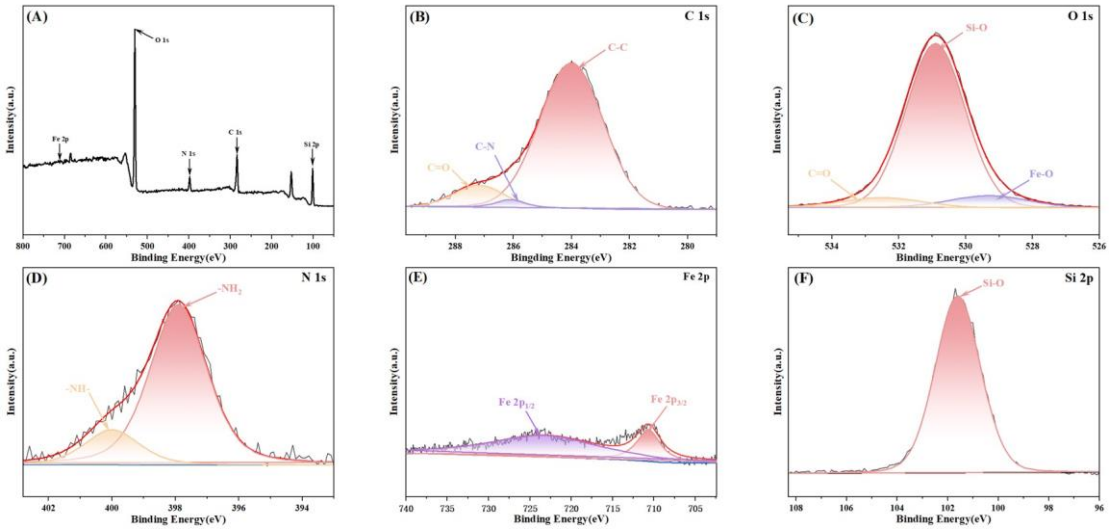


Fig.3. (A) Full range XPS spectrum of MPG-2 particles; (B)- (F) local magnification spectra of C 1s, O 1s, N 1s, Fe 2p and Si 2p, respectively.

3.2 Effect of different generation on immobilization of laccase

As illustrated in Table 1, there is an observed increase in the content of C and N elements within the carrier as the generation progresses. In principle, one would expect the concentration of the N element to rise exponentially with the augmentation in the number of generations. However, the practical concentration of this element diverges from the anticipated exponential increase, attributable to steric impediments encountered during the synthesis procedure (36). With advancing generations, the potential for grafting additional amino groups onto the carrier surface escalates, thereby offering an increased number of immobilization sites. Notwithstanding, the

loading of laccase did not exhibit a significant upsurge from MPG-2 to MPG-3, due to steric constraints encountered during the immobilization process. As a result, MPG-2 was designated as the preferred immobilized carrier for laccase (32).

Table 1. Elemental composition analysis of MPG-x and its loading capacity.

Sample	N content (%)	C content (%)	Laccase loading (mg/g)
MPG-0	0.15	0.29	32.4 ± 2.1
MPG-1	0.38	0.58	43.5 ± 1.6
MPG-2	0.53	0.84	48.9 ± 0.9
MPG-3	0.61	0.95	50.7 ± 1.1

3.3 Optimization of immobilized laccase conditions

The optimization of the laccase immobilization process involved several key parameters: cross-linking agent concentration, immobilization time, initial laccase concentration, pH, temperature, and the concentration of Cu^{2+}. As illustrated in Fig. 4(A), both the loading capacity and activity of laccase increased with the rise in glutaraldehyde concentration, peaking at 1% (v/v). Beyond this concentration, however, overcrosslinking and the inherent toxicity of glutaraldehyde led to a decline in both loading capacity and enzyme activity (32). Fig.4(B) demonstrates that as immobilization time increased, more laccase was loaded onto the carrier, reaching maximum loading and activity after 3 hours. Further extension of immobilization time did not enhance loading due to the limited binding sites on the carrier surface and resulted in decreased activity from excessive cross-linking. According to Fig. 4(C), increasing the amount of added laccase enhanced both loading and activity until the optimal addition of 0.7 mL/mL was reached. Beyond this point, although more laccase could be immobilized, its activity diminished due to excessive aggregation on the carrier surface, leading to steric hindrance that impeded full contact between laccase and substrate (37). Additionally, pH and temperature were critical factors affecting laccase immobilization. Fig.4(D) and Fig.4(E) showed that laccase activity peaked at pH 3.0 and 30°C, beyond which excessive alkalinity or elevated temperatures could

damage the protein structure of laccase. As depicted in Fig.4(F), the laccase activity attained its peak when the concentration of Cu^{2+} was 0.07 M.

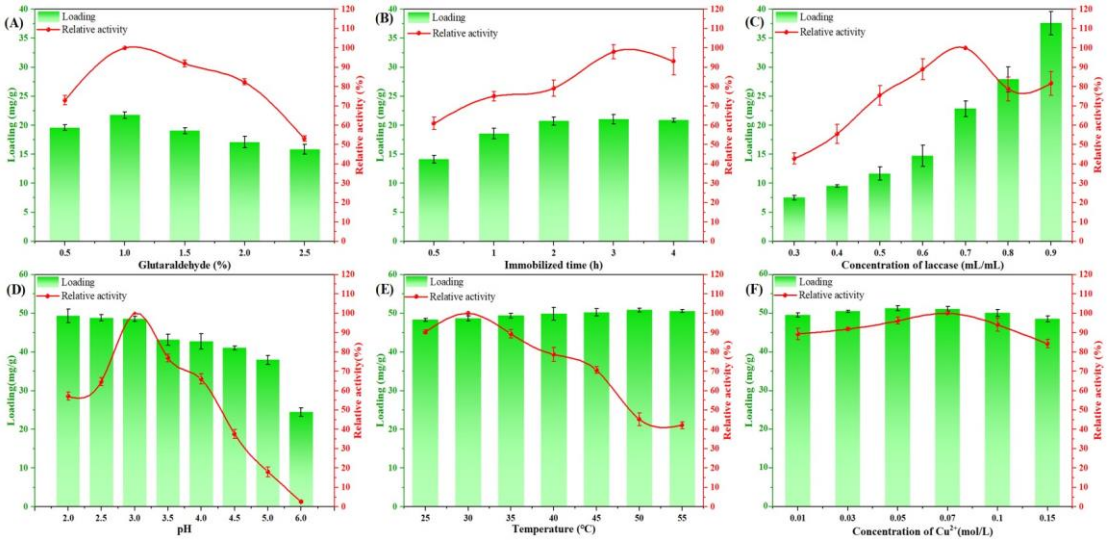


Fig.4. Effects of glutaraldehyde concentration (A), immobilized time (B), concentration of laccase (C), pH (D), temperature (E) and concentration of Cu^{2+} (F) on laccase loading and relative activity.

As illustrated in Table 2, under the optimal immobilization conditions, the laccase loading of MPG-2@GA-Lac and MPG-2@Cu^{2+}-Lac was determined to be 48.9 mg/g and 50.6 mg/g, respectively. Correspondingly, the immobilization efficiencies were recorded at 77.5% and 80.4%, respectively. The incorporation of the transition metal ion Cu^{2+} did not markedly enhance the laccase loading capacity, potentially attributable to the restricted number of binding sites on the surface of the immobilized carrier. Nonetheless, Cu^{2+} was found to activate the active site of laccase, thereby improving the activity of the immobilized laccase compared to GA, as evidenced by the increased activity recovery from 74.4% to 108.1% (38).

Table 2 The immobilization capacity of carriers and the activity of immobilized laccase. [a]

362

	Laccase immobilization	Laccase activity			
Carrier	Immobilization efficiency (%)	Laccase loading (mg/g)	Expressed activity (U/g biocatalyst)	Specific activity (U/g protein)	Activity retention (%)
MPG-2@GA-Lac	77.5±1.6	48.9±0.9	56.8±2.1	1158.7±42.9	74.4±2.8
MPG-2@Cu^{2+}-Lac	80.4±1.7	50.6±1.1	82.5±1.5	1683.1±29.6	108.1±1.9

363 [a] represent the protein content of free laccase is 178 mg/L, and the activity of free
364 laccase is 1557.8 U/g protein.

365 **3.4 Stability of free laccase and immobilized laccase**

366 In this study, the stability of immobilized laccase and free laccase at different pH
367 and temperature, thermal stability at 50 ℃ and reusability were studied to evaluate the
368 performance of immobilized laccase.

369 Fig.5(A) showed that the optimal temperature for free laccase and
370 MPG-2@GA-Lac was 50 ℃, whereas for MPG-2@Cu^{2+}-Lac was 40 ℃. Between 25 ℃
371 and 50 ℃, the molecular thermal movement of free laccase increased the contact
372 between the laccase and the substrate, and thus showed higher laccase activity (31).
373 When the temperature increased from 50 ℃ to 65 ℃, the laccase activity decreased
374 rapidly because the protein structure was destroyed at high temperature. When the
375 temperature reached 65 ℃, the relative activity of free laccase was only 21.6%.
376 However, due to the protective effect of the carrier, MPG-2@GA-Lac still had 48.6%
377 relative activity at 65 ℃. MPG-2@Cu^{2+}-Lac had strong binding with laccase due to

the presence of transition metal ion Cu^{2+}, which helped to further stabilize the conformation of laccase, and thus exhibits better relative activity than free laccase and MPG-2@GA-Lac at a wider temperature range (38). The relative activity of MPG-2@Cu^{2+}-Lac could still reach 58.4% at 65 ℃.

As shown in Fig.5(B), the optimal pH of free laccase was 2.5, while that of MPG-2@GA-Lac and MPG-2@Cu^{2+}-Lac was 3.0. However, both MPG-2@GA-Lac and MPG-2@Cu^{2+}-Lac showed higher activity in a wide range of pH, because the immobilized carriers could better protect the conformation of laccase, thus reducing the effect of pH on laccase. When pH was greater than 3.0, the relative activity of free laccase was lower than that of MPG-2@GA-Lac, and when pH=5.5, the relative activity of free laccase was 13.7%, while that of MPG-2@GA-Lac and MPG-2@Cu^{2+}-Lac were 24.4% and 26.1%, respectively.

Fig.5(C) showed the residual relative activity of MPG-2@GA-Lac and MPG-2@Cu^{2+}-Lac after 10 cycles. After repeated use for 5 cycles, the relative activities of MPG-2@GA-Lac and MPG-2@Cu^{2+}-Lac were 84.2% and 87.1%, respectively. After 10 cycles, the relative activity of MPG-2@GA-Lac and MPG-2@Cu^{2+}-Lac were 66.4% and 70.2%. Both immobilized laccase showed excellent recycling performance.

Fig.5(D) showed the thermal stability of free laccase and two immobilized laccase at 50 ℃ and different time. After 1 h heat treatment, the relative activity of free laccase was 32.0%, that of MPG-2@GA-Lac decreased to 64.4%, but that of MPG-2@Cu^{2+}-Lac decreased by 16.7% only. After 5 h of heat treatment, the free laccase was basically inactivated, while the relative activity of MPG-2@GA-Lac and MPG-2@Cu^{2+}-Lac remained 20.3% and 39.32%, respectively. This indicated that the presence of immobilized carrier could protect the structure of laccase at high temperature, and the introduction of copper ions further stabilizes the spatial conformation of laccase itself.

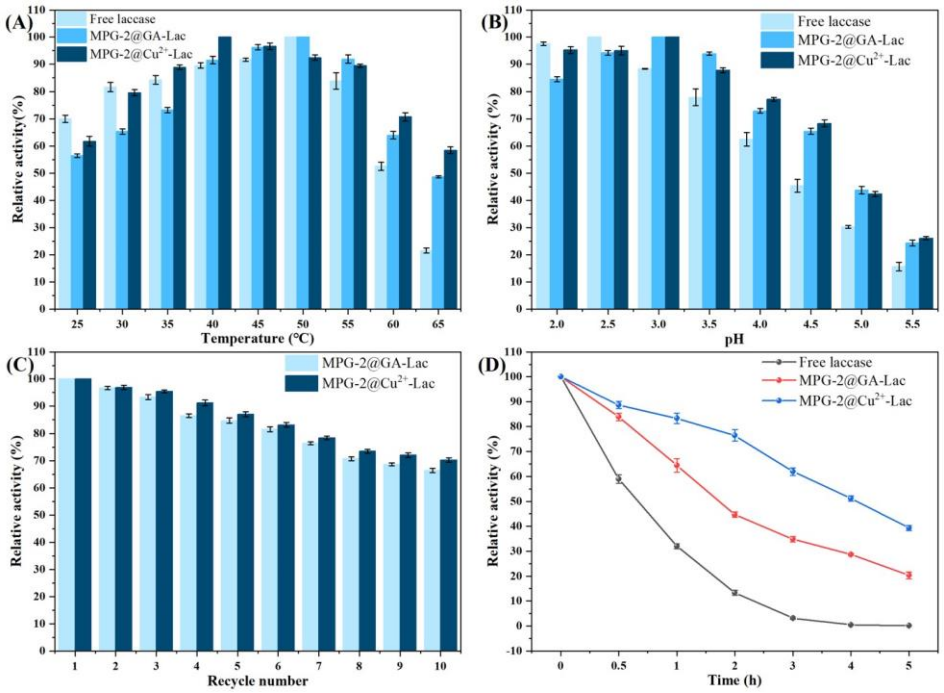


Fig.5. Temperature stability (A), pH stability (B) and thermal stability at 50 ℃ (D) of free laccase, MPG-2@GA-Lac and MPG-2@Cu^{2+}-Lac. Reusability of MPG-2@GA-Lac and MPG-2@Cu^{2+}-Lac (C).

The storage stability of laccase before and after immobilization was examined by placing free laccase and immobilized laccase at 4 ℃ for a duration of 22 days. The initial activity was defined as 100%. As depicted in Fig. 6, following 22 days of storage, the activity of free laccase diminished by more than half, with only 37.5% of the relative activity remaining. Conversely, MPG-2@GA-Lac and MPG-2@Cu^{2+}-Lac exhibited high activity even after 22 days, retaining 70.4% and 91.2% of the initial activity, respectively. These findings indicate that the immobilized carrier can effectively protect laccase and mitigate the loss of enzyme activity. Moreover, it was observed that the introduction of Cu^{2+} could further safeguard the spatial structure of laccase, thereby significantly reducing the loss of laccase activity (38).

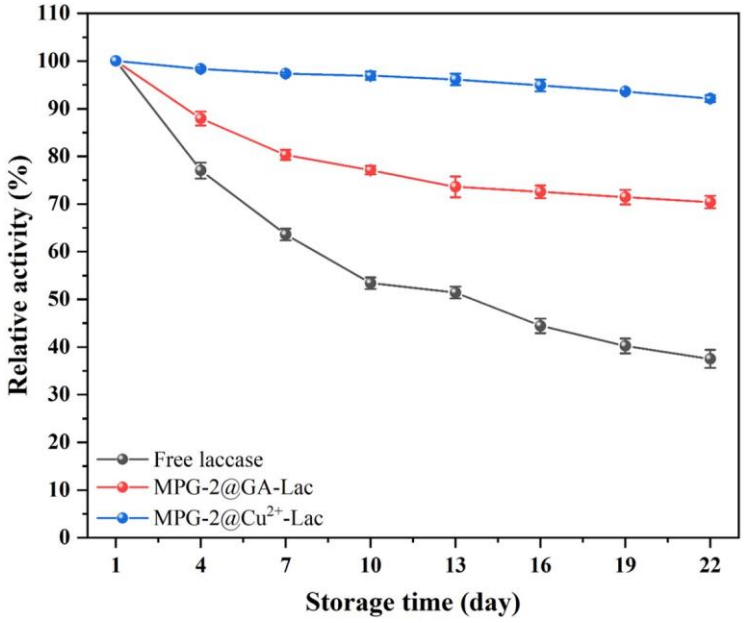


Fig.6. The Impact of Storage Duration on the Activity of Free Laccase (pH=2.5, 4 °C) and Immobilized Laccase.

3.5 Effects of parameters on MO removal

As a crucial factor influencing laccase activity, pH has a direct impact on the ultimate degradation of MO. As presented in Fig. 7, an investigation was conducted into the MO removal capabilities of free laccase, MPG - 2@GA - Lac, and MPG - 2@Cu^{2+}-Lac at different pH values.

As depicted in Fig. 7(A-E), free laccase demonstrated a rapid MO removal efficiency owing to its direct interaction with MO. At pH = 2.0 and pH = 6.0, the MO removal efficiency of free laccase reached 53.25% and 48.95%, respectively, 40 minutes later, the removal efficiency tended towards equilibrium. After 3 hours, the MO removal efficiencies were 57.05% and 50.22%, respectively.

In the case of immobilized laccase, due to the protective effect of the carrier, the contact efficiency between laccase and the substrate was lower than that of free laccase. Consequently, the MO removal efficiency of immobilized laccase gradually increased with the extension of treatment time. When the pH increased from 2.0 to 3.0, the removal efficiency of immobilized laccase for MO improved gradually. At pH = 3.0, both MPG - 2@GA - Lac and MPG - 2@Cu^{2+}-Lac achieved their optimal MO removal

efficiencies after 3 hours, which were 73.13% and 82.56%, respectively. However, as the pH increased, the MO removal efficiencies of MPG - 2@GA - Lac and MPG - 2@Cu^{2+}-Lac began to decline. At pH = 6.0, the MO removal efficiencies of MPG - 2@GA - Lac and MPG - 2@Cu^{2+}-Lac after 3 hours dropped to 65.88% and 68.5%, respectively, which were still 1.31 and 1.36 times higher than that of free laccase. This could be attributed to the fact that laccase was merely immobilized on the surface of the carrier and could still be directly exposed to the MO solution in a neutral environment, consistent with the results of the pH stability shown in Fig. 5(B). The results presented in Fig. 7 indicate that immobilized laccase can effectively enhance the MO removal efficiency of free laccase within the pH range under consideration.

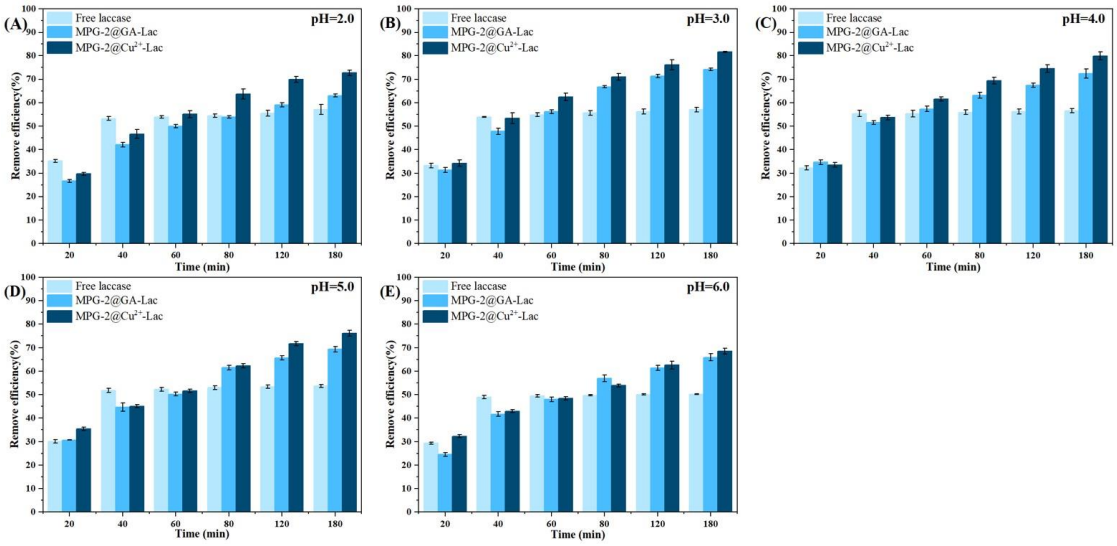


Fig.7. (A)-(E) Effects of free laccase, MPG-2@GA-Lac and MPG-2@Cu^{2+}-Lac on MO removal under different pH conditions (40 ℃, Initial MO concentration 10mg/L).

Temperature emerged as a pivotal factor influencing the expression of laccase activity. Consequently, the removal efficacy of MO by free laccase, MPG-2@GA-Lac, and MPG-2@Cu^{2+}-Lac across varying temperatures was also investigated, as illustrated in Fig. 8. The findings revealed that the efficiency of MO removal by both free laccase (within the initial 40 minutes) and immobilized laccase (within the initial 60 minutes) exhibited a direct correlation with temperature. This phenomenon can be attributed to the facilitation of molecular thermal motion in a suitable high-temperature

environment, thereby accelerating the removal of MO (39). The removal efficiency of MO by free laccase neared equilibrium after 40 minutes, with the optimal removal efficiency reaching 63.33% after 3 hours. The removal efficiency of MO by immobilized laccases MPG-2@GA-Lac and MPG-2@Cu^{2+}-Lac demonstrated an increasing trend with rising temperature. Upon attaining 40 ℃, both MPG-2@GA-Lac and MPG-2@Cu^{2+}-Lac achieved their peak MO removal efficiencies after 3 hours, which were 72.8% and 82.45%, respectively. However, protracted exposure to elevated temperatures led to a decline in laccase activity, resulting in reduced MO removal efficiency. Notwithstanding, even at 55 ℃, the MO removal efficiencies for MPG-2@GA-Lac and MPG-2@Cu^{2+}-Lac remained at 64.51% and 68.4% after 3 hours, respectively. The results presented in Fig. 8 indicated that immobilized laccase could demonstrate superior MO removal capabilities across a broader temperature range compared to free laccase.

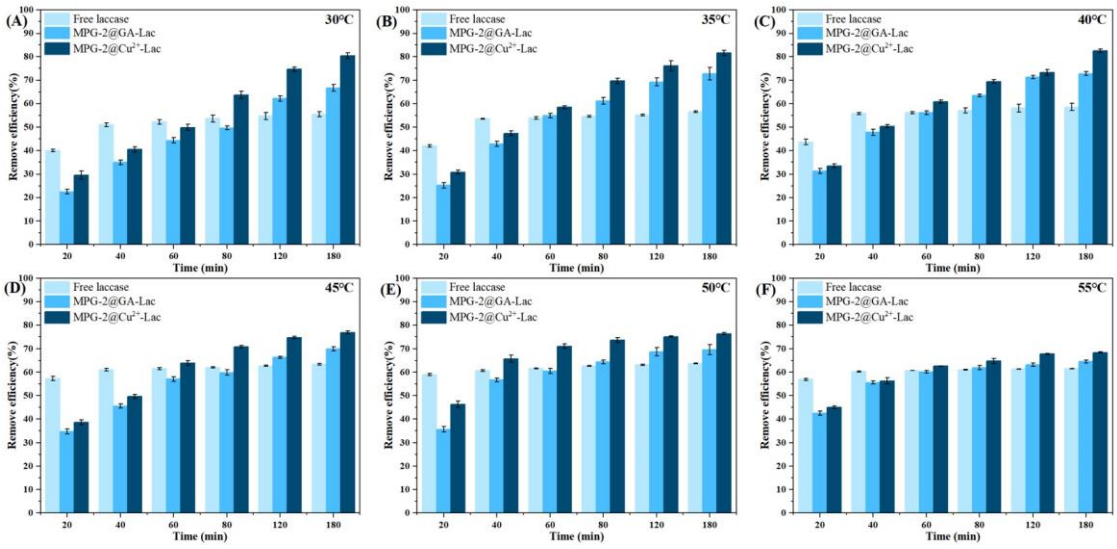


Fig.8. (A)-(F) Effects of free laccase, MPG-2@GA-Lac and MPG-2@Cu^{2+}-Lac on MO removal at different temperatures (free laccase reaction pH=2.5, immobilized laccase reaction pH=3.0, initial MO concentration 10 mg/L).

Finally, the impact of free laccase, as well as immobilized laccase MPG-2@GA-Lac and MPG-2@Cu^{2+}-Lac, on the removal of MO was examined by modulating the initial MO concentration, which ranged from 10 mg/L to 50 mg/L. The outcomes are presented in Fig. 9. It was observed that the removal efficiency of MO by

free laccase, MPG-2@GA-Lac, and MPG-2@Cu^{2+}-Lac diminished as the initial MO concentration increased. At an initial MO concentration of 10 mg/L, the removal efficiency after 6 hours for free laccase, MPG-2@GA-Lac, and MPG-2@Cu^{2+}-Lac were 59.68%, 74.55%, and 82.94%, respectively. As the MO concentration rose, the removal efficiency for all three decreased. Specifically, when the initial MO concentration for free laccase was 50 mg/L, the removal efficiency after 6 hours dropped to 30.92% due to the toxic influence of MO dye on the biological enzyme. In contrast, the immobilized laccase's activity was less affected by MO due to the protective carrier. Consequently, even at an initial MO concentration of 50 mg/L, MPG-2@GA-Lac and MPG-2@Cu^{2+}-Lac achieved removal efficiencies of 63.23% and 69.23% after 6 hours, respectively, which is 2.04 and 2.24 times higher than that of free laccase. These findings underscore the advantages of immobilized laccase.

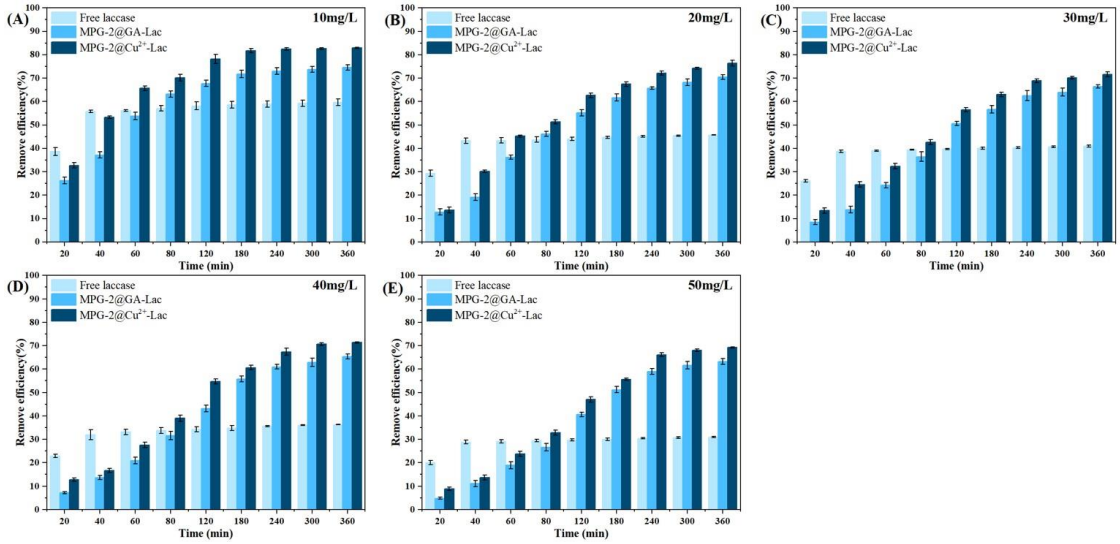


Fig.9. (A)-(E) Effects of free laccase, MPG-2@GA-Lac and MPG-2@Cu^{2+}-Lac on MO removal at different initial MO concentrations (free laccase reaction pH=2.5, immobilized laccase reaction pH=3.0, reaction temperature 40 °C).

Collectively, these results demonstrate that the MO removal efficiency of immobilized laccase surpasses that of free laccase across varying pH levels, temperatures, and initial MO concentrations.

In addition, a systematic investigation was conducted on the degradation kinetics of two immobilized laccases, namely MPG-2@GA-Lac and MPG-2@Cu^{2+}-Lac.

Subsequently, the degradation kinetics curves of these two immobilized laccases for MO under diverse conditions were determined. As illustrated in Fig.10(A, D), pH exerts an influence on the surface charge properties of the immobilized laccase, thereby impacting the degradation efficiency. The degradation rate constants of MPG-2@GA-Lac and MPG-2@Cu^{2+}-Lac were found to be favorable within a neutral to slightly acidic environment. With the ascending of pH, the degradation rate constants initially increased and subsequently decreased, reaching their maximum at pH=3.0. The respective degradation rate constants K_{obs} were 0.030 and 0.033. An appropriate pH can enhance the microenvironment of the laccase, thereby augmenting the expression of laccase activity and the efficiency of MO degradation.

A more detailed examination was carried out to explore the effect of temperature on the degradation efficiency of MO, and the corresponding results are presented in Fig.10(B, E). As the temperature rose, the degradation efficiency of the two immobilized laccases also increased. MPG-2@GA-Lac and MPG-2@Cu^{2+}-Lac attained their peak degradation rates at 55 ℃, with degradation rate constants K_{obs} of 0.054 and 0.058, respectively. This may be attributed to the fact that high temperature accelerates the movement of MO molecules, thereby enhancing the contact between MO and the immobilized laccase.

Finally, the effect of initial MO concentration on the degradation efficiency of immobilized laccase was investigated. The results were shown in Fig.10(E, F). The degradation efficiency of MO by MPG-2@GA-Lac and MPG-2@Cu^{2+}-Lac diminished as the initial MO concentration increased. At the initial MO concentration of 10 mg/L, the maximum degradation rate constants of MPG-2@GA-Lac and MPG-2@Cu^{2+}-Lac were 0.0245 and 0.0265, respectively. When the concentration of MO increased to 50 mg/L, the degradation efficiency decreased significantly (with the degradation rate constants dropping to 0.0067 and 0.0074, respectively), which indicated that high concentration of MO might competitively inhibit the active sites of laccase, thus affecting the interaction between substrate and laccase (40). Nevertheless, the results

indicated that both MPG-2@GA-Lac and MPG-2@Cu^{2+}-Lac maintained a removal rate of MO exceeding 60%.

The results demonstrate that MPG-2@Cu^{2+}-Lac displayed a significantly enhanced degradation efficiency in comparison to MPG-2@GA-Lac. It is postulated that Cu^{2+}, serving as a crucial component of the active site of laccase, not only safeguards the conformational integrity of laccase under adverse conditions, but also engages in the electron exchange between laccase and the substrate (41).

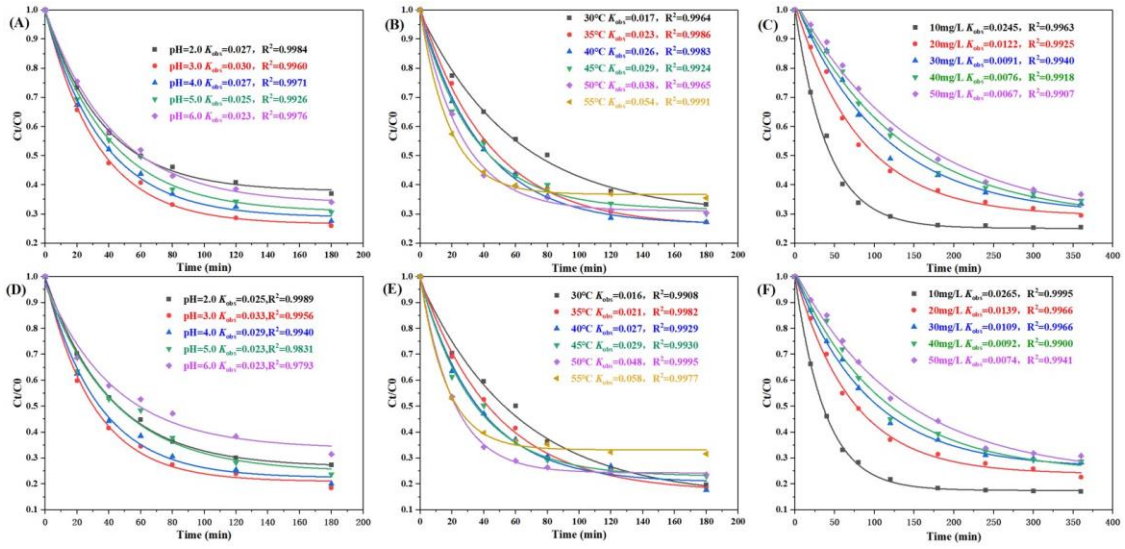


Fig.10. The degradation kinetics curve of MO for MPG-2@GA-Lac (A - C) and MPG-2@Cu^{2+}-Lac (D - F) under various pH values, temperatures, and initial MO concentrations.

Under the optimally defined degradation conditions, MPG-2@Cu^{2+}-Lac demonstrated a superior removal efficiency (9.43%) for methylene blue (MO) compared to MPG-2@GA-Lac, as illustrated in Fig.11(A). This observation may be ascribed to the synergistic interaction between metal ions and laccase, which accelerates the catalytic reaction, thereby enhancing the removal efficiency of MO (38, 42). Furthermore, it can be observed from Fig.11(A) that the carrier MPG-2 exhibited minimal adsorptive capacity for MO, suggesting that the removal process primarily depends on the enzymatic degradation mediated by laccase.

3.6 Reusability for removal of MO

The reusability of immobilized laccase in the dye degradation process is a critical

parameter for assessing the performance of the immobilized laccase system. Therefore, this study investigated the cyclic degradation performance of MPG-2@GA-Lac and MPG-2@Cu^{2+}-Lac under the optimal conditions (pH 3.0, 40 ℃), as depicted in Fig.11(B). After six cycles of operation, the removal efficiency of MO by MPG-2@GA-Lac and MPG-2@Cu^{2+}-Lac decreased to 58.48% and 66.18%, respectively. This decline may be attributed to the shedding of laccase over successive cycles or the inhibitory effects resulting from substrate toxicity (40, 42). These findings collectively indicate that the immobilized laccase system possesses considerable reusability.

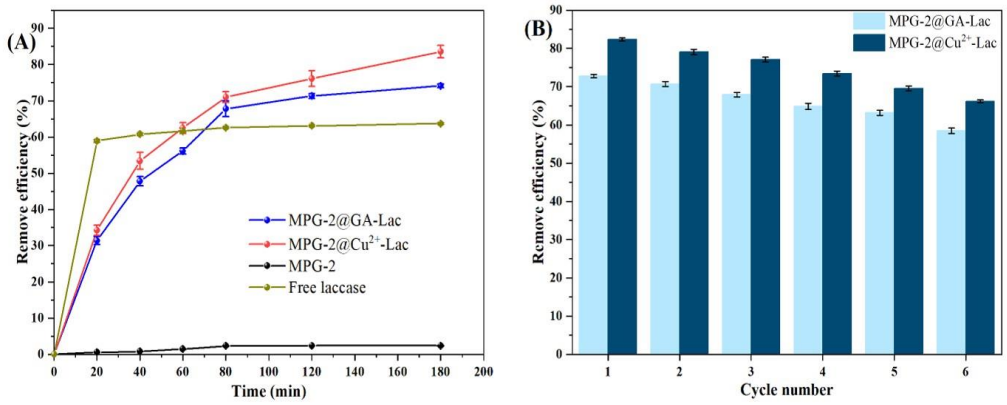


Fig.11. (A) remove efficiency of MPG-2@Cu^{2+}-Lac and MPG-2@GA-Lac (initial MO concentration 10 mg/L, 40 ℃, pH=3.0). (B) reusability of MPG-2@GA-Lac and MPG-2@Cu^{2+}-Lac.

4. CONCLUSION

In this study, the surface of Fe_3O_4 nanoparticles was successfully functionalized with polyamidoamine (PAMAM) dendrimers through an amino-functionalization process employing a divergent approach. Following optimization, the optimal immobilization carrier was identified as the magnetic dendrimer (MPG-2), which was grafted with the second-generation PAMAM dendrimers. Two immobilized laccase preparations, MPG-2@GA-Lac and MPG-2@Cu^{2+}-Lac, were fabricated via glutaraldehyde cross-linking and cupric ion chelate adsorption, respectively, achieving laccase loadings of 48.9 mg/g and 50.6 mg/g. The corresponding activity recoveries

were 74.4% and 108.1%, respectively. These results demonstrated that MPG-2@GA-Lac and MPG-2@Cu^{2+}-Lac exhibited enhanced stability compared to free laccase. The removal efficiencies of MPG-2@GA-Lac and MPG-2@Cu^{2+}-Lac for 10 mg/L of methylene blue (MO) reached 72.19% and 82.56%, respectively, after 3 hours. Following six cycles of degradation, the removal efficiencies were maintained at 58.48% and 66.18%, respectively. The incorporation of Cu^{2+} significantly improved the stability of the immobilized laccase system and the removal efficiency of MO. The immobilized laccase system developed in this study exhibited a favorable removal effect on MO, indicating a broad application potential in the degradation of dye wastewater.

AUTHORSHIP CONTRIBUTION STATEMENT

Tianwen Lu: Conceptualization, Investigation, Data curation, Writing-original draft. **Yixuan Dai:** Software. **Yue Shi:** Software. **Xiaojun Wang:** Validation, Visualization. **Yinan Hong：** Software, Conceptualization. **Hong Pan:** Investigation, Validation, Supervision, Writing-review & editing. **Zhansheng Wu**: Editing the draft.

Funding Declaration

This work was supported by the Special Scientific Research Program of the Department of Education of Shaanxi Province (22JK0399).

Ethics declaration

Not applicable.

References

1. **Backes, E., Kato, C. G., Corrêa, R. C. G., Moreira, R. d. F. P. M., Peralta, R. A., Barros, L., Ferreira, I. C., Zanin, G. M., Bracht, A., and Peralta, R. M**.: Laccases in food processing: Current status, bottlenecks and perspectives, Trends Food

601 Sci Technol, 115, 445-460 (2021).
602 2. **Kadam, A. A., Saratale, G. D., Ghodake, G. S., Saratale, R. G., Shahzad, A.,**
603 **Magotra, V. K., Kumar, M., Palem, R. R., and Sung, J.-S**.: Recent advances in the
604 development of laccase-based biosensors via nano-immobilization techniques,
605 Chemosensors, 10, 58 (2022).
606 3. **Yavaser, R. and Karagözler, A. A.:** Laccase immobilized
607 polyacrylamide-alginate cryogel: A candidate for treatment of effluents, Process
608 Biochemistry, **101**, 137-146 (2021).
609 4. **Mao, G., Wang, K., Wang, F., Li, H., Zhang, H., Xie, H., Wang, Z., Wang, F.,**
610 **and Song, A.:** An engineered thermostable laccase with great ability to decolorize and
611 detoxify malachite green, Int J Mol Sci, **22**, 11755 (2021).
612 5. **Sharma, A., Jain, K. K., Srivastava, A., Shrivastava, B., Thakur, V. V., Jain,**
613 **R., and Kuhad, R.:** Potential of in situ SSF laccase produced from Ganoderma
614 lucidum RCK 2011 in biobleaching of paper pulp, Bioprocess Biosyst Eng, **42**,
615 367-377 (2019).
616 6. **Datta, S., Veena, R., Samuel, M. S., and Selvarajan, E.:** Immobilization of
617 laccases and applications for the detection and remediation of pollutants: a review,
618 Environ Chem Lett, **19**, 521-538 (2021).
619 7. **Wang, D. and Jiang, W.:** Preparation of chitosan-based nanoparticles for enzyme
620 immobilization, Int J Biol Macromol, **126**, 1125-1132 (2019).
621 8. **Yang, B., Tang, K., Wei, S., Zhai, X., and Nie, N.:** Preparation of functionalized
622 mesoporous silica as a novel carrier and immobilization of laccase, Applied
623 Biochemistry and Biotechnology, **193**, 2547-2566 (2021).
624 9. **Costa, J. B., Lima, M. J., Sampaio, M. J., Neves, M. C., Faria, J. L.,**
625 **Morales-Torres, S., Tavares, A. P., and Silva, C. G.:** Enhanced biocatalytic
626 sustainability of laccase by immobilization on functionalized carbon
627 nanotubes/polysulfone membranes, Chemical Engineering Journal, **355**, 974-985
628 (2019).

10. **Huang, W., Zhang, W., Gan, Y., Yang, J., and Zhang, S.:** Laccase immobilization with metal-organic frameworks: Current status, remaining challenges and future perspectives, Critical Reviews in Environmental Science and Technology, **52**, 1282-1324 (2022).

11. **Li, R., Li, X., Tian, D., Liu, X., and Wu, Z.:** Amino-functionalized MOF immobilized laccase for enhancing enzyme activity stability and degrading Congo red, Journal of the Taiwan Institute of Chemical Engineers, **143**, 104647 (2023).

12. **Feng, J., Huang, Q.-Y., Zhang, C., Ramakrishna, S., and Dong, Y.-B.:** Review of covalent organic frameworks for enzyme immobilization: Strategies, applications, and prospects, International Journal of Biological Macromolecules, **248**, 125729 (2023).

13. **Lin, J., Wen, Q., Chen, S., Le, X., Zhou, X., and Huang, L.:** Synthesis of amine-functionalized Fe_3O_4@ C nanoparticles for laccase immobilization, International journal of biological macromolecules, **96**, 377-383 (2017).

14. **Fan, Y., Ke, C., Su, F., Li, K., and Yan, Y.:** Various types of lipases immobilized on dendrimer-functionalized magnetic nanocomposite and application in biodiesel preparation, Energy & Fuels, **31**, 4372-4381 (2017).

15. **Chen, Z., Yao, J., Ma, B., Liu, B., Kim, J., Li, H., Zhu, X., Zhao, C., and Amde, M.:** A robust biocatalyst based on laccase immobilized superparamagnetic Fe_3O_4@ SiO_2–NH_2 nanoparticles and its application for degradation of chlorophenols, Chemosphere, **291**, 132727 (2022).

16. **Ran, F., Zou, Y., Xu, Y., Liu, X., and Zhang, H.:** Fe3O4@ MoS2@ PEI-facilitated enzyme tethering for efficient removal of persistent organic pollutants in water, Chemical Engineering Journal, **375**, 121947 (2019).

17. **Li, Z., Chen, Z., Zhu, Q., Song, J., Li, S., and Liu, X.:** Improved performance of immobilized laccase on Fe_3O_4@ C-Cu^{2+} nanoparticles and its application for biodegradation of dyes, Journal of Hazardous Materials, **399**, 123088 (2020).

18. **Najafi, F., Salami-Kalajahi, M., and Roghani-Mamaqani, H.:** A review on

657 synthesis and applications of dendrimers, Journal of the Iranian Chemical Society, **18**,
658 503-517 (2021).
659 19. **Wong, K. H., Guo, Z., Law, M.-K., and Chen, M.:** Functionalized PAMAM
660 constructed nanosystems for biomacromolecule delivery, Biomaterials Science, **11**,
661 1589-1606 (2023).
662 20. **Guizze, F., Serra, C. H. R., and Giarolla, J.:** PAMAM Dendrimers: A review of
663 methodologies employed in biopharmaceutical classification, Journal of
664 Pharmaceutical Sciences, **111**, 2662-2673 (2022).
665 21. Rabiee, N., Ahmadvand, S., Ahmadi, S., Fatahi, Y., Dinarvand, R., Bagherzadeh,
666 M., Rabiee, M., Tahriri, M., Tayebi, L., and Hamblin, M. R.: Carbosilane dendrimers:
667 Drug and gene delivery applications, Journal of Drug Delivery Science and
668 Technology, 59, 101879 (2020).
669 22. **Saluja, V., Mishra, Y., Mishra, V., Giri, N., and Nayak, P.:** Dendrimers based
670 cancer nanotheranostics: An overview, International journal of pharmaceutics, **600**,
671 120485 (2021).
672 23. **Wang, Y., Luo, Y., Zhao, Q., Wang, Z., Xu, Z., and Jia, X.:** An
673 enzyme-responsive nanogel carrier based on PAMAM dendrimers for drug delivery,
674 ACS applied materials & interfaces, **8**, 19899-19906 (2016).
675 24. **Zhao, P., Tian, L., Li, X., Ali, Z., Zhang, B., Zhang, H., and Zhang, Q.:** Effect
676 of the structure and length of flexible chains on dendrimers grafted Fe_3O_4@
677 SiO_2/PAMAM magnetic nanocarriers for lipase immobilization, ACS Sustainable
678 Chemistry & Engineering, **4**, 6382-6390 (2016).
679 25. **Fan, X., Lin, D., Xu, Z., and Li, Y.:** Pd/Cu bimetallic catalyst immobilized on
680 PEI capped cellulose-polyamidoamine dendrimer: Synthesis, characterization, and
681 application in Sonogashira reactions for the synthesis of alkynes and benzofurans,
682 Colloids and Surfaces A: Physicochemical and Engineering Aspects, **648**, 129206
683 (2022).
684 26. **Sohail, I., Bhatti, I. A., Ashar, A., Sarim, F. M., Mohsin, M., Naveed, R., Yasir,**

685 **M., Iqbal, M., and Nazir, A.:** Polyamidoamine (PAMAM) dendrimers synthesis,
686 characterization and adsorptive removal of nickel ions from aqueous solution, Journal
687 of Materials Research and Technology, **9**, 498-506 (2020).
688 27. **Chen, Z., Yao, J., Knudsen, T. Š., Ma, B., Liu, B., Li, H., Zhu, X., Zhao, C.,**
689 **Pang, W., and Cao, Y.:** Degradation of novel mineral flotation reagent
690 8-hydroxyquinoline by superparamagnetic immobilized laccase: Effect, mechanism
691 and toxicity evaluation, Chemical Engineering Journal, **432**, 134239 (2022).
692 28. **Unniganapathi, B. V. and Mohanan Puzhavoorparambil, V.:** Development of
693 PAMAM dendrimer-modified magnetic chitosan: a novel platform for α-amylase
694 immobilization, Polymer Bulletin, 1-18 (2022).
695 29. **Xia, T.-T., Liu, C.-Z., Hu, J.-H., and Guo, C.:** Improved performance of
696 immobilized laccase on amine-functioned magnetic Fe_3O_4 nanoparticles modified with
697 polyethylenimine, Chemical Engineering Journal, **295**, 201-206 (2016).
698 30. **Li, X., Wu, Z., Tao, X., Li, R., Tian, D., and Liu, X.:** Gentle one-step
699 co-precipitation to synthesize bimetallic CoCu-MOF immobilized laccase for boosting
700 enzyme stability and Congo red removal, Journal of Hazardous Materials, **438**, 129525
701 (2022).
702 31. **Qiu, X., Wang, S., Miao, S., Suo, H., Xu, H., and Hu, Y.:** Co-immobilization of
703 laccase and ABTS onto amino-functionalized ionic liquid-modified magnetic chitosan
704 nanoparticles for pollutants removal, Journal of hazardous materials, **401**, 123353
705 (2021).
706 32. **He, S., Xu, B., Liu, Y., Yin, X., Yang, W., and Chen, Y.:** Immobilization of
707 laccase on PAMAM dendrimers modified core-shell Fe_3O_4-SiO_2 magnetic composite
708 particles for degradation of 2, 4-dichlorophenol, Colloids and Surfaces A:
709 Physicochemical and Engineering Aspects, **679**, 132606 (2023).
710 33. **Sheikh, S., Nasseri, M. A., Chahkandi, M., Allahresani, A., and Reiser, O.:**
711 Functionalized magnetic PAMAM dendrimer as an efficient nanocatalyst for a new
712 synthetic strategy of xanthene pigments, Journal of Hazardous Materials, **400**, 122985

(2020).

34. **Zhu, W., Zhang, Y., Hou, C., Pan, D., He, J., and Zhu, H.:** Covalent immobilization of lipases on monodisperse magnetic microspheres modified with PAMAM-dendrimer, Journal of Nanoparticle Research, **18**, 1-13 (2016).

35. **Liu, Y., Wang, Y., Zhou, S., Lou, S., Yuan, L., Gao, T., Wu, X., Shi, X., and Wang, K.:** Synthesis of high saturation magnetization superparamagnetic Fe_3O_4 hollow microspheres for swift chromium removal, ACS Applied Materials & Interfaces, **4**, 4913-4920 (2012).

36. **Tsubokawa, N., Ichioka, H., Satoh, T., Hayashi, S., and Fujiki, K.:** Grafting of 'dendrimer-like'highly branched polymer onto ultrafine silica surface, Reactive and functional polymers, **37**, 75-82 (1998).

37. **Shan, H., Wang, X., Ge, Y., and Li, Z.:** Homologous amino acids promoted co-immobilization of laccase and mediator onto geopolymer microspheres for enhancing degradation of dyes in water, Journal of Hazardous Materials, **423**, 127107 (2022).

38. **Feng, P., Tao, X., Li, W., Chen, Y., Tian, F., Zhu, L., Liu, X., and Wu, Z.:** Enhancement of photocatalytic performance of cu-decorated bifunctional g-C3N4-laccase ICPB system, Applied Surface Science, **654**, 159381 (2024).

39. **Qiu, X., Wang, Y., Xue, Y., Li, W., and Hu, Y.:** Laccase immobilized on magnetic nanoparticles modified by amino-functionalized ionic liquid via dialdehyde starch for phenolic compounds biodegradation, Chemical Engineering Journal, **391**, 123564 (2020).

40. **Yang, X., Chen, X., Wang, H., Cavaco-Paulo, A., and Su, J.:** Co-immobilizing laccase-mediator system by in-situ synthesis of MOF in PVA hydrogels for enhanced laccase stability and dye decolorization efficiency, Journal of Environmental Management, **353**, 120114 (2024).

41. **Olshansky, Y., Masaphy, S., Root, R. A., and Rytwo, G.:** Immobilization of Rhus vernicifera laccase on sepiolite; effect of chitosan and copper modification on

laccase adsorption and activity, Applied Clay Science, **152**, 143-147 (2018).

42. **Jia, J., Xue, P., Ma, L., Li, P., and Xu, C.:** Deep degradation of atrazine in water using co-immobilized laccase-1-hydroxybenzotriazole-Pd as composite biocatalyst, Journal of Hazardous Materials, **468**, 133779 (2024).

Author names and affiliations:

Tianwen Lu:

School of Environmental and Chemical Engineering, Xi'an Polytechnic University, Xi'an 710048, China, E-mail: 20185345@163.com

Yixuan Dai:

School of Environmental and Chemical Engineering, Xi'an Polytechnic University, Xi'an 710048, China, E-mail: 223454863@qq.com

Yue Shi:

School of Environmental and Chemical Engineering, Xi'an Polytechnic University, Xi'an 710048, China, E-mail: 1246353306@qq.com

Hong Pan:

School of Environmental and Chemical Engineering, Xi'an Polytechnic University, Xi'an 710048, China, E-mail: 441595837@qq.com

Xiaojun Wang:

School of Environmental and Chemical Engineering, Xi'an Polytechnic University, Xi'an 710048, China, E-mail: 316411156@qq.com

Yinan Hong:

School of Environmental and Chemical Engineering, Xi'an Polytechnic University, Xi'an 710048, China, E-mail: 20180389@xpu.edu.cn

Zhansheng Wu:

School of Environmental and Chemical Engineering, Xi'an Polytechnic University, Xi'an 710048, China, E-mail: 376682156@qq.com

Corresponding author

Hong Pan:

School of Environmental and Chemical Engineering, Xi'an Polytechnic University, Xi'an 710048, China, E-mail:441595837@qq.com